

Application of Oxygen Eddy Correlation in Aquatic Systems

CLAUDIA LORRAI

Eawag, Surface Waters—Research and Management, Kastanienbaum, and Institute of Biogeochemistry and Pollutant Dynamics, ETH Zurich, Zurich, Switzerland

DANIEL F. MCGINNIS*

Eawag, Surface Waters—Research and Management, Kastanienbaum, Switzerland

PETER BERG

Department of Environmental Sciences, University of Virginia, Charlottesville, Virginia

ANDREAS BRAND⁺

Eawag, Surface Waters—Research and Management, Switzerland

ALFRED WÜEST

Eawag, Surface Waters—Research and Management, Kastanienbaum, and Institute of Biogeochemistry and Pollutant Dynamics, ETH Zurich, Zurich, Switzerland

(Manuscript received 14 July 2009, in final form 4 January 2010)

ABSTRACT

The eddy correlation technique is rapidly becoming an established method for resolving dissolved oxygen fluxes in natural aquatic systems. This direct and noninvasive determination of oxygen fluxes close to the sediment by simultaneously measuring the velocity and the dissolved oxygen fluctuations has considerable advantages compared to traditional methods. This paper describes the measurement principle and analyzes the spatial and temporal scales of those fluctuations as a function of turbulence levels. The magnitudes and spectral structure of the expected fluctuations provide the required sensor specifications and define practical boundary conditions for the eddy correlation instrumentation and its deployment. In addition, data analysis and spectral corrections are proposed for the usual nonideal conditions, such as the time shift between the sensor pair and the limited frequency response of the oxygen sensor. The consistency of the eddy correlation measurements in a riverine reservoir has been confirmed—observing a night–day transition from oxygen respiration to net oxygen production, ranging from -20 to $+5$ $\text{mmol m}^{-2} \text{day}^{-1}$ —by comparing two physically independent, eddy correlation instruments deployed side by side. The natural variability of the fluctuations calls for at least ~ 1 h of flux data record to achieve a relative accuracy of better than $\sim 20\%$. Although various aspects still need improvement, eddy correlation is seen as a promising and soon-to-be widely applied method in natural waters.

* Current affiliation: IFM-GEOMAR, Leibniz Institute of Marine Sciences at the University of Kiel, East Shore Campus, Kiel, Germany.

⁺ Current affiliation: University of California, Berkeley, Berkeley, California.

Corresponding author address: Claudia Lorrai, Eawag, Surface Waters—Research and Management, Seestrasse 79, CH-6047 Kastanienbaum, Switzerland.
E-mail: claudia.lorrai@eawag.ch

1. Introduction

Measuring turbulent transport of dissolved substances in aquatic environments is crucial for understanding biogeochemical and physical processes and their interactions. Dissolved oxygen (DO) fluxes are especially of interest and therefore key for the understanding of aquatic systems, as it is a major component of aquatic system functioning and related biogeochemical processes.

DO fluxes within the water column are often experimentally determined by balancing rates of changes within layers of water masses (Emerson et al. 2002). However, complex motions and in situ DO consumption make it challenging to accurately perform such balances. An alternative method to estimate DO fluxes is using eddy diffusivities determined by other means (such as by heat budgets, microstructure measurements, or turbulence modeling) and multiplying them with the local DO gradients. However, all of these methods are often not adequate for applications in naturally complex settings. The DO flux into the sediment, referred to as the sediment uptake rate, is often resolved with invasive methods, such as benthic chambers or in situ microprofiles. However, both methods are limited in that they either alter or exclude the natural hydrodynamic regime (benthic chambers), or that interpreting microprofiles and estimating the fluxes can be partly arbitrary.

The aquatic application of the eddy correlation (EC) technique alleviates many of those shortcomings and provides the possibility to quantify DO fluxes in a direct manner. The technique is widely used in the atmospheric boundary layer but is relatively new for aquatic systems. So far Berg et al. (2003, 2007), Berg and Huettel (2008), and Kuwae et al. (2006) used the EC technique to determine DO fluxes over coastal marine sediments. Berg et al. (2009) deployed the EC device also in the deep ocean, whereas McGinnis et al. (2008) and Brand et al. (2008) studied DO flux dynamics in a riverine reservoir and a freshwater seiche-driven lake, respectively.

Since Berg et al. (2003) first tested the EC technique by combining oxygen microsensor and acoustic velocimeter measurements, experience and confidence have increased with respect to instrumentation, deployment, and data analysis. The outstanding advantage of the EC technique is the potential to record undisturbed fluxes with high temporal and spatial resolution. By correlating the vertical velocity fluctuations w' with the fluctuations C' of the constituent of interest, the instantaneous exchange flux can be calculated in a straightforward manner. The average $\overline{w'C'}$ yields the net flux directed toward (respiration) or away from (production) the sediment.

With this paper, we document the acquired experience with EC. After introducing the background, we provide an analysis of the expected temporal and spatial scales of the flux-relevant velocity and DO fluctuations in lakes/reservoirs and oceans. Furthermore, we list the technical requirements and instrument specifications for resolving these scales and provide a systematic guide for deployment and data analysis. We propose appropriate filtering and frequency response correction techniques

as well as useful indications for practical application. Finally, we test for the first time the reproducibility of the aquatic EC technique by comparing fluxes measured with two independent EC devices deployed side by side in a run-of-river reservoir.

2. Requirements for resolving the flux-relevant scales

a. Background and assumptions

The EC technique implies that the turbulent scalar fluctuations C' (e.g., DO) and the current fluctuations $u'_1, u'_2, u'_3 = w'$ are simultaneously resolved in order to determine the temporal average of the covariance $\overline{u'_j C'}$ (i.e., turbulent flux of property C in direction u_j). To deduce the covariance $\overline{u'_j C'}$, the critical step is to separate the two fluctuations from the two means of the collected time series. This challenge is illustrated in Fig. 1 showing time series of vertical velocity w , DO concentrations C , and the corresponding instantaneous fluxes $w'C'(t)$ calculated by subtraction from the respective means [$w'(t) = w(t) - \overline{w}(t)$ and $C'(t) = C(t) - \overline{C}(t)$].

Concentrations and their fluxes are related by the three-dimensional ($j = 1, 2, 3$) conservation equation, balancing the rate of change of quantity C with the divergence and convergence of those fluxes and the sources/sinks of property C :

$$\frac{\partial \overline{C}}{\partial t} + \sum_j \overline{u'_j} \frac{\partial \overline{C}}{\partial x_j} = D_c \sum_j \frac{\partial^2 \overline{C}}{\partial x_j^2} + S_c - \sum_j \frac{\partial (\overline{u'_j C'})}{\partial x_j}. \quad (1)$$

The terms represent the local rate of change of concentration C (storage term), divergence of the advective (mean) flux, molecular diffusion ($D_c =$ molecular diffusion coefficient) of C , sum of sources and/or sinks S_c , and divergence of turbulent flux, respectively.

Assuming slowly changing mean concentrations \overline{C} , Eq. (1) can be simplified. This has been formulated by Taylor (1938) in his frozen-field hypothesis that turbulent eddies should not significantly change their properties when passing by the measurement point. This assumption implies that the eddy time scale τ_E has to be longer than the time needed for turbulent eddies to pass the measurement scale L ($\tau_E > L/u$). Or, more generally stated, the changes of the background flow $[(\partial u/\partial x), (\partial u/\partial t)]$ are small compared to the dynamics of passing eddies $[(\partial u'/\partial x), (\partial u'/\partial t)]$. Hence, with the EC technique, only the flux in the final term of Eq. (1) is observed.

As the EC technique for aquatic systems is still developing, it is realistic to assume for the near future that it will mainly be applied to less complex settings such as

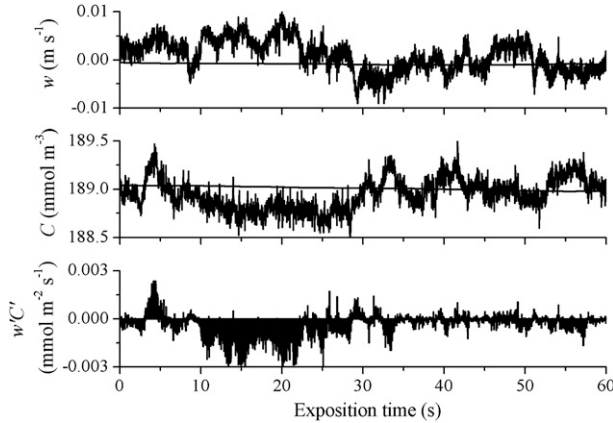


FIG. 1. Time series of (top) vertical velocity w , (middle) DO concentration C , and (bottom) instantaneous flux $w'C'$. The slowly varying horizontal lines are running averages (window length ~ 5 min). Data series taken on 25 May 2007 in Lake Wohlensee, Switzerland.

in boundary layers. There, the ideal conditions for measuring vertical fluxes require (i) horizontal and homogeneous flows (zero divergence) and (ii) only gradual/slow changes of the background concentration C (quasi stationary). The diffusion term can be ignored, except in the diffusive boundary layer, where molecular transport dominates. Hence, the integration of Eq. (1) leads to the mass balance at height h above the sediment water interface ($z = 0$) of

$$\overline{w'C'}(h) = \overline{w'C'}(0) + \int_0^h S_C(z) dz. \quad (2)$$

Equation (2) implies that the flux measured at height h is equal to the flux through the interface plus the integrated sources and/or sinks over the water column of thickness h . If the measurements are close to the interface (h is small), or if S_C is weak, then the measured flux is equal to the interface flux:

$$\overline{w'C'}(h) \approx \overline{w'C'}(0). \quad (3)$$

Separation of turbulent fluctuations from the background mean at the study site is usually not well-defined and necessitates a careful analysis of the relevant scales, in particular of the cospectrum of the measured fluctuations.

b. Characteristic scales

Ideally for EC, the variance-preserving spectrum would show a distinct spectral gap (a range of low energy content) that separates the advective (large) scales associated with the mean flow from the turbulent (small) scales, as is often observed for wind spectra measured in the planetary boundary layer (Van der Hoven 1957). In

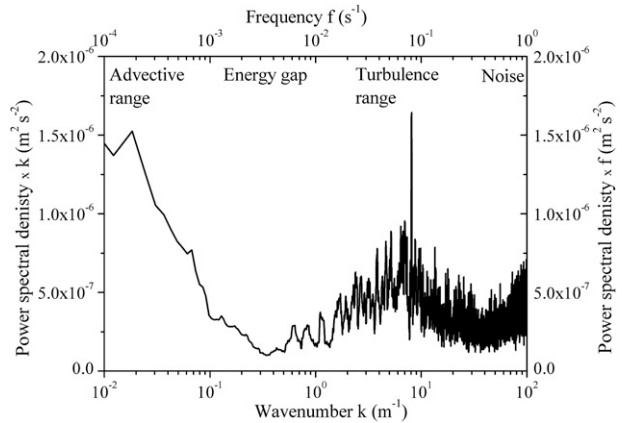


FIG. 2. Variance-preserving spectrum of current (downstream component) in frequency and wavenumber domain for an average longitudinal velocity $u = 0.01 \text{ m s}^{-1}$. ADV data was recorded in Lake Alpnach on 27–28 Aug 2007 at a depth of 23 m (0.1 m above sediment). The advective range is clearly separated from the turbulent range by a prominent energy gap. Not all spectra show such a favorable separation of the three ranges.

Fig. 2 an example of the variance-preserving spectrum in the wavenumber and frequency domain is shown for the downstream current velocity component measured in a bottom boundary layer (BBL) of a lake 0.1 m above the sediment. In natural waters, unfortunately, there is often no obvious spectral gap that separates the large-scale advective motions from the small-scale eddies (McGinnis et al. 2008). Therefore, a major challenge with the EC technique is the separation of turbulent fluctuations (higher frequency range) from advective motions (lower frequency range) and, thus, to resolve the complete turbulent flux cospectrum $\text{Co}_{wC}(f)$ of vertical velocity w' and of the tracer concentration C' . Expressed in formal terms, this flux cospectrum yields (Stull 1988)

$$\overline{w'C'} = \int_0^\infty \text{Co}_{wC}(f) df. \quad (4)$$

An analysis of spatial and temporal scales provides the requirements for the EC hardware. In Table 1 the relevant scales for measurements are exemplified for low turbulence systems, characterized by the horizontal velocity at 1 m above sediment U_{1m} , such as lakes or the deep sea ($U_{1m} = 0.02 \text{ m s}^{-1}$), and high turbulence regions, such as the coastal ocean ($U_{1m} = 0.20 \text{ m s}^{-1}$). The upper bound time scale for largest eddies (τ_{LE}) at the measurement location $h = 0.1$ m above the sediment is given by $\tau_{LE} = h/u_*$, where the friction velocity is $u_* = (C_{1m})^{1/2} U_{1m}$ with bottom drag coefficient C_{1m} at 1 m above the sediment. The horizontal velocity at a measurement height 0.1 m is calculated by applying the law

TABLE 1. Scale-analysis for two typical turbulence levels in the BBL of natural waters. The smallest a priori fluctuations of vertical velocity and DO concentration for oligotrophic, mesotrophic, and eutrophic aquatic system are compared.

Property	Symbol	Low turbulence	High turbulence
		$U_{1m} = 0.02 \text{ m s}^{-1}$	$U_{1m} = 0.2 \text{ m s}^{-1}$
Boundary conditions			
Bottom drag coefficient	C_{1m}	0.0025	0.0025
Friction velocity	$u_* = (C_{1m})^{1/2} U_{1m}$	0.001 m s^{-1}	0.01 m s^{-1}
Kinematic viscosity (10°C)	ν	$1.3 \times 10^{-6} \text{ m}^2 \text{ s}^{-1}$	$1.3 \times 10^{-6} \text{ m}^2 \text{ s}^{-1}$
Molecular diffusion coefficient for DO (10°C)	D	$1.3 \times 10^{-9} \text{ m}^2 \text{ s}^{-1}$	$1.3 \times 10^{-9} \text{ m}^2 \text{ s}^{-1}$
Characteristic scales			
Height above sediment = length scale largest eddies	h	0.1 m	0.1 m
Horizontal velocity	$U_{0.1m}$	0.014 m s^{-1}	0.14 m s^{-1}
Energy dissipation	$\varepsilon = u_*^3 / \kappa h$	$2.4 \times 10^{-8} \text{ W kg}^{-1}$	$2.4 \times 10^{-5} \text{ W kg}^{-1}$
Timescale largest eddies	$\tau_{LE} = h/u_*$	100 s	10 s
Inertial time scale*	$\tau_N = 1/N$		
- Weak stability	$N^2 = 10^{-6} \text{ s}^{-2}$	1000 s	1000 s
- Strong stability	$N^2 = 10^{-4} \text{ s}^{-2}$	100 s	100 s
Kolmogorov scale (smallest eddies)	$L_K = 2\pi(\nu^3/\varepsilon)^{1/4}$	0.02 m	0.003 m
Timescale smallest eddies	$\tau_K = (L_K^2/\varepsilon)^{1/3}$	7.4 s	0.2 s
Batchelor (diffusive) scale	$L_B = 2\pi(\nu D^2/\varepsilon)^{1/4}$	$6.2 \times 10^{-4} \text{ m}$	$1.1 \times 10^{-4} \text{ m}$
Smallest fluctuations of vertical velocity (w') and BBL DO concentration (C')			
Vertical velocity fluctuations u_*		0.001 m s^{-1}	0.01 m s^{-1}
Oligotrophic DO fluxes ($<10 \text{ mmol m}^{-2} \text{ day}^{-1}$)		$\sim 0.12 \text{ mmol m}^{-3}$	$\sim 0.012 \text{ mmol m}^{-3}$
Mesotrophic DO fluxes ($10 \text{ to } 30 \text{ mmol m}^{-2} \text{ day}^{-1}$)		$\sim 0.23 \text{ mmol m}^{-3}$	$\sim 0.023 \text{ mmol m}^{-3}$
Eutrophic DO fluxes ($>30 \text{ mmol m}^{-2} \text{ day}^{-1}$)		$\sim 0.35 \text{ mmol m}^{-3}$	$\sim 0.035 \text{ mmol m}^{-3}$

* Away from the BBL in the thermocline the representative scale is the Ozmidov length scale. For strong stratification ($N^2 \approx 10^{-4} \text{ s}^{-2}$) the scale ranges from centimeters ($\varepsilon \approx 10^{-11} \text{ W kg}^{-1}$) to decimeters ($\varepsilon \approx 10^{-9} \text{ W kg}^{-1}$) and for weak stratification ($N^2 \approx 10^{-8} \text{ s}^{-2}$) from meters ($\varepsilon \approx 10^{-11} \text{ W kg}^{-1}$) to a few tens of meters ($\varepsilon \approx 10^{-9} \text{ W kg}^{-1}$), respectively (Wüest and Lorke 2003).

of the wall. In the stratified interior (away from the BBL) the Ozmidov length scale characterizes the vertical extent of eddies that can still overturn depending on the stratification expressed as the water column stability N^2 (Table 1). The corresponding inertial time scale of these overturns is given by N^{-1} . The high frequency cutoff of the turbulent spectrum is determined by the Kolmogorov length scale $L_K = 2\pi(\nu^3/\varepsilon)^{1/4}$ characterizing the dissipative range in a fluid of dissipation ε and of kinematic viscosity ν (Kolmogorov 1941). The time scale of the smallest eddies is $\tau_K = (L_K^2/\varepsilon)^{1/3}$ (Table 1). The Batchelor scale, defined as $L_B = 2\pi(\nu D^2/\varepsilon)^{1/4}$ where D is the molecular diffusion coefficient of oxygen, is listed for completeness. The diffusive scale is not contributing to the DO flux because the vertical velocity fluctuations are eliminated at L_K .

These scales must be interpreted as order of magnitude quantities for upper and lower bounds of the complete turbulence spectrum. However, the intrinsic time scales shown in Table 1 are not the scales we see with an

Eulerian measurement approach. Fixed point measurements register frozen turbulence structures advected passed the sensor, rather than the intrinsic time evolution of an eddy.

The expected turbulent DO fluctuations in natural waters depend on the local DO gradients and turbulence. As typical DO fluxes in the BBL are known for a given trophic status, the magnitude of DO fluctuations can be estimated based on the turbulent velocities (Table 1). Typical fluctuations are listed in Table 1 for oligotrophic ($<10 \text{ mmol m}^{-2} \text{ day}^{-1}$), mesotrophic ($10\text{--}30 \text{ mmol m}^{-2} \text{ day}^{-1}$) or eutrophic water bodies ($>30 \text{ mmol m}^{-2} \text{ day}^{-1}$; Redfield 1958; Vollenweider 1975). Assuming, that the turbulence is well developed, the friction velocity u_* is a valuable proxy for the vertical velocity fluctuations w' (Table 1) and the anticipated DO fluctuations C' can be estimated based on Eq. (5)

$$C'_{\text{exp}} \approx \frac{\overline{w'C'}}{u_*}. \quad (5)$$

For low turbulence we expect the vertical velocity fluctuations on the order of $u_* = 0.001 \text{ m s}^{-1}$ and the characteristic DO concentration fluctuations C'_{exp} vary depending on the trophic status from 0.12 mmol m^{-3} (oligotrophic) to 0.35 mmol m^{-3} (eutrophic; Table 1). For high turbulence, u_* is approximately 0.01 m s^{-1} and the DO concentration fluctuations range from 0.012 to $0.035 \text{ mmol m}^{-3}$ (Table 1). These ranges give the framework for the expected sensor resolutions.

c. Sensor requirements

Ideal EC measurements require instruments that are able to adequately resolve the complete cospectrum of the fluctuations, w' and C' (Table 1). There are two principal obstacles to overcome: First, the sensors inherently modify the “true” cospectrum by specific (empirical) frequency-dependent transfer functions, $H^2_{\text{sensors}}(f)$, which account for the nonperfect sensor properties (Mudge and Lueck 1994; Gregg 1999). For example, to correct for the frequency response of sensors, the measured cospectrum $\text{Co}_{wC,\text{meas}}(f)$ can be back-corrected (Eugster and Senn 1995; Horst 2000), and the turbulent flux is integrated over the corrected cospectrum by

$$\overline{(w'C')} = \int_0^\infty H_{wC}^{-2}(f) \text{Co}_{wC,\text{meas}}(f) df. \quad (6)$$

Second, all sensors have a lower- (lb) and upper-bound (ub) frequency limit within which their signals are physically meaningful. Beyond these limits, noise of several forms mask the sensor signals and affect the covariance in Eq. (6). If the limits and the associated “lost” covariance at both ends of the cospectrum can be estimated by empirical approximations, $\text{extrap}(f)$, then the best estimate for the total covariance is given by all three contributions:

$$\begin{aligned} \overline{(w'C')} = & \int_0^{\text{lb}} \text{extrap}(f) df + \int_{\text{lb}}^{\text{ub}} H_{wC}^{-2}(f) \text{Co}_{wC,\text{meas}}(f) df \\ & + \int_{\text{ub}}^\infty \text{extrap}(f) df. \end{aligned} \quad (7)$$

The flux-relevant frequency range extends typically over ~ 2 to ~ 3 orders of magnitude (Fig. 2), calling for a broad sensitive range of the sensors (Baldocchi 2003). Under ideal conditions, the sensor range covers more than 90% of the flux-containing spectrum in Eq. (7), such that the uncertainty due to extrapolating the covariance beyond lb and ub becomes small. In atmospheric EC measurements, $\text{extrap}(f)$ is often known because of universal forms of $\text{Co}_{wC}(f)$ (Kaimal et al. 1972). Once such functions also become available for

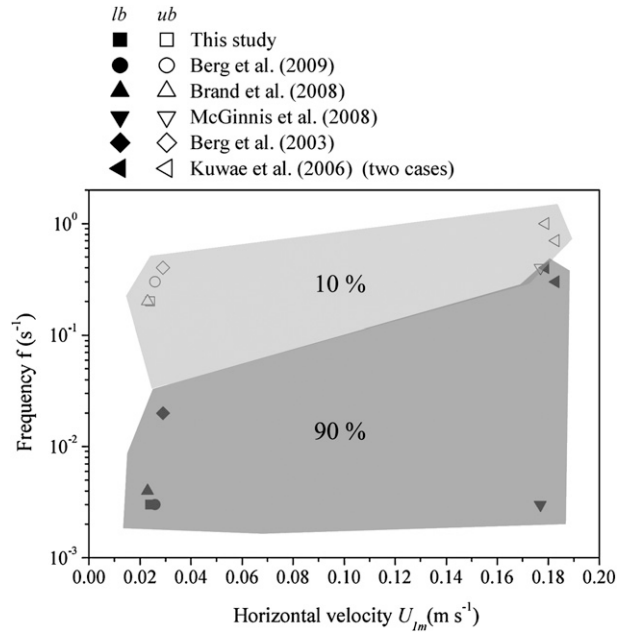


FIG. 3. Frequency bands taken from cumulative cospectra of all DO EC publications including this study. The dark shaded area and the black symbols represent the frequency, at which 90% (lower frequency bound) of the flux is included. The light shaded area and the white symbols represent the frequency at which 10% (upper frequency bound) of the flux is contributed.

aquatic systems, the two corrections in Eq. (7) become straightforward. In Fig. 3 the flux-relevant frequency range for all EC DO-flux measurements performed so far are plotted as a function of the horizontal velocity U_{1m} . The white and black symbols mark the frequencies where the contributions to the DO flux reach 10% and 90%, respectively. The data for these upper- and lower-bound frequencies in Fig. 3 are extracted from DO flux measurements in coastal ocean and inland waters. The high frequency limit ranges from $\sim 1 \text{ s}^{-1}$ (coastal ocean) to $\sim 0.2 \text{ s}^{-1}$ (lakes) and the lower bound varies from $\sim 0.5 \text{ s}^{-1}$ (coastal ocean) to $\sim 0.003 \text{ s}^{-1}$ (lakes). The frequency range reported in Kuwae et al. (2006) may not be typical for coastal oceans in general, as the relatively narrow frequency bands are caused by the shallow site ($\sim 0.40 \text{ m}$ depth, limiting the size of the largest eddies) and the dominance of the surface waves. Based on the analysis provided in Table 1, the DO and velocimeter sensors (including their electronics) should fulfill the following requirements.

1) RELATIVE PRECISION

The velocity and DO sensors should resolve differences of less than 0.001 m s^{-1} and $0.012 \text{ mmol m}^{-3}$ (Table 1) in order to detect the smallest expected (natural) fluctuations.

With a modern 16-bit analog-to-digital converter, the resolution of the output does not limit the precision (Mudge and Lueck 1994). As the mean values of w and C are removed in the EC calculations, absolute accuracy is not important compared to the relative precision, characterized by reproducibility (detailed below) and low drift.

2) SENSOR DYNAMICS AND SAMPLING

The shortest time scales of flux-contributing eddies (Table 1) generally range between 1 s (lowland streams, ocean) to 10 s (lakes, reservoirs). Therefore, aquatic EC measurements require a sampling rate at least twice the maximum frequency of the signal (1 s^{-1}), and sensor response faster than 1 s. The attenuation of the high-frequency contributions of the cospectrum can be corrected by using the transfer function for two sensors (Horst 2000)

$$H_{wC}^2 = \frac{(1 + \omega^2 \tau_w \tau_C) + \omega(\tau_w - \tau_C)Q/Co}{(1 + \omega^2 \tau_w^2)(1 + \omega^2 \tau_C^2)}, \quad (8)$$

where $\omega = 2\pi f$, Co is the covariance spectrum, Q is the quadrature spectrum, τ_w is the $1/e$ response time of the velocity measurement device and τ_C the $1/e$ sensor response time for scalar C (here, DO). For the case of a fast velocity sensor ($\tau_w \approx 0$) and a slow DO sensor, the transfer function simplifies to $H_{wC}^2(f) = [1 + (2\pi f \tau_C)^2]^{-1}$ (Eugster and Senn 1995; Horst 2000), where τ_C is the $1/e$ response time of the DO sensor (Gregg 1999).

In the low-frequency range (largest eddies), sensor drift is more likely to introduce artificial contributions. The lower limit (lb) in the frequency range has to be determined empirically (details in section 3). However, an approximate integration time can be calculated from the variance of the $w'C'$ histogram (Fig. 4). The covariance $w'C'$ has higher relative scatter than the individual fluctuations w' and C' . Therefore, a longer time interval is required for a robust average covariance $w'C'$ compared to the time interval needed to obtain the same relative accuracy for the averages of w and C . For the example of a typical flux histogram shown in Fig. 4 and by assuming a Laplace distribution, $\overline{w'C'}$ is $-3.3 \times 10^{-5} \text{ mmol m}^{-2} \text{ s}^{-1}$ and the variance σ^2 equals $1.6 \times 10^{-7} \text{ mmol}^2 \text{ m}^{-4} \text{ s}^{-2}$. Error analysis provides the measurement duration (or number of samples) necessary to reduce the error of the statistical average of $w'C'$ (characterized by σ^2) below the target relative accuracy (a) as $f^{-1}[\sigma^2/(a \overline{w'C'})^2]$. For a prescribed relative accuracy of $a = 20\%$ and a measurement frequency $f = 1 \text{ s}^{-1}$, a measurement duration of at least $\sim 1 \text{ h}$ is required (Fig. 4). In addition, the measurement duration should be several times (~ 5 to 10) the eddy time scale

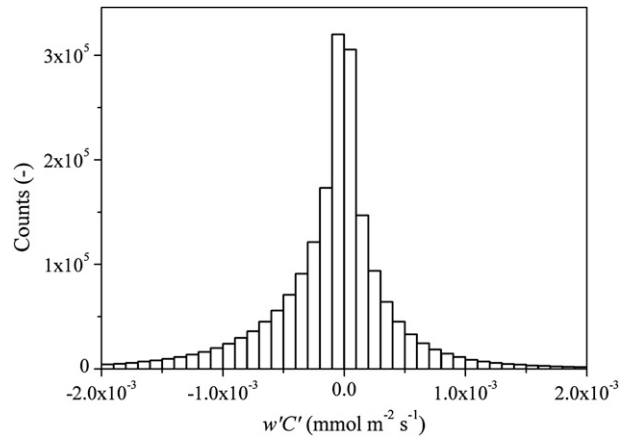


FIG. 4. Histogram of $\sim 30\,000$ instantaneous $w'C'(t)$ fluxes (Fig. 1, lower panel) estimated at 1 s^{-1} . The mean of the assumed Laplace distribution is $-3.3 \times 10^{-5} \text{ mmol m}^{-2} \text{ s}^{-1}$ with a variance of $\sigma^2 = 1.6 \times 10^{-7} \text{ mmol}^2 \text{ m}^{-4} \text{ s}^{-2}$.

(Businger 1986). For the values considered in Table 1, the duration would be $\sim 15 \text{ min}$. Thus, in our example (a typical lacustrine BBL) a flux-averaging time ranging from 15 min to 1 h is ideal.

d. Deployment considerations

When deploying the EC equipment aboard a frame, the orientation must be such that the legs do not cause flow distortion or generate fluctuations registered in the sampling volume. The frame should be rigid enough to avoid frame vibrations and have suitably large feet to prevent sinking.

The velocity measurement volume should be small enough to resolve the smallest eddies contributing to the fluxes (Table 1). Furthermore, to ensure the data pairs are correlated, it is important that the DO sensor is close to the velocity measurement volume. Therefore, the distance between the DO sensor tip (point measurement) and the velocity measurement volume (acoustic signals are reflected from particles within a cylindrical sampling volume, section 3) should be less apart than ~ 10 times the Kolmogorov scale (Table 1); the closer to the sampling volume the less time-shift correction is required. The synchronization of the two signals is important, although technically not difficult for the frequency ranges considered (see below).

The DO gradient is generally stronger near the sediment and therefore fluctuations are more easily detected. In addition to the sediment roughness and water depth, the measurement height above the sediment (in our case between 10 and 15 cm), determines the horizontal footprint, which is defined as the area that contributes (e.g., 90%) to the flux (Berg et al. 2007).

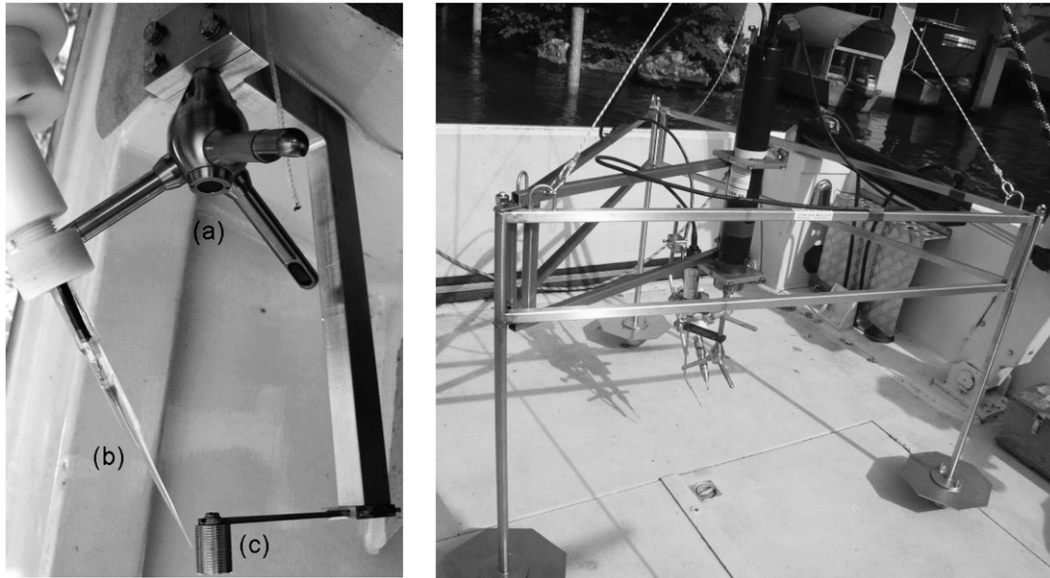


FIG. 5. (left) Closeup of (b) the DO sensor positioned close to (c) the metal cylinder 15 cm below (a) the ADV transducer. (right) Eddy correlation frame with ADV and sensors mounted.

3. Implementation of EC measurements and data analysis

a. Instrumentation: The realization of an EC device

The EC device includes a Clark-type microelectrode oxygen sensor (Unisense AS, Denmark) and an acoustic Doppler velocimeter (ADV; “Vector”) customized to allow their coupling (Nortek AS, Norway). With the simultaneous recording of velocity and DO data within the ADV, synchronization problems are avoided. The ADV samples velocities internally at a rate between 100 and 250 Hz and outputs averaged velocity at a rate from 1 to 64 Hz. The analog DO input signal is sampled at the same output rate. To deploy the EC device, we use a tripod based on Berg and Huettel (2008) and manufactured by Rovelli SA (Switzerland; Fig. 5, right).

The ADV measures velocity in three dimensions in a user-selected cylindrical volume (from 0.4 to 1.4 cm³) of 10-mm diameter and variable height. The favorable properties of the ADV include (i) no calibration, (ii) wide measurement range (horizontal velocity: ~ 0.001 up to ~ 8 m s⁻¹), and (iii) precision of 1% of the velocity range selected. Depending on the particle concentration in the water, a smaller volume is preferable as it allows covariance estimates at smaller scales and is therefore better suited for complete resolution of the upper end of the spectrum (Table 1; Fig. 2). The downside of the smallest sampling volume is the increasing noise due to less frequent sampling of the transmit pulse and lower number of particles, which increases the uncertainty. Before deployment, the electrode is positioned close to

the ADV’s measurement volume by using a temporarily mounted positioning frame (Fig. 5, left) as a guide.

The fast DO electrode, with a tip diameter of 10 μ m, has a 90% response time of less than 0.2 s and a detection limit measured under laboratory conditions in DO depleted water of ~ 0.15 mmol m⁻³ (L. R. Damgaard, Unisense, 2008, personal communication). Submerged instruments are usually less affected by noise and reach potentially lower detection limits.

The DO electrode must be polarized (-0.8 V) for a minimum of 2 h before deployment. In addition to standard DO calibration, we record DO with a simultaneously deployed DO logger (e.g., DO optode), which provides a continuous reference measurement and the possibility for correcting sensor drift.

The current (picoamperes) from the DO microelectrode is converted to a potential difference (volts) before amplification by a low-noise current-to-voltage converter prior to a custom designed instrumentation amplifier in series with a guard circuit (C. Dinkel, Eawag, 2009, personal communication; the schematic is available upon request). The capacitor in the converter acts as a passive low-pass filter that reduces noise and the risk of aliasing, which refers to the artificial signal produced if the original signal is not sampled with at least twice the highest frequency of the original signal. Capacitors, unfortunately, also increase the DO signal response time. Capacitances ranging from 33 up to 4700 pF were tested for frequency response and noise. For comparing the tests, vertical velocity and DO signal have been low-pass filtered at 1 Hz before estimating the standard deviation

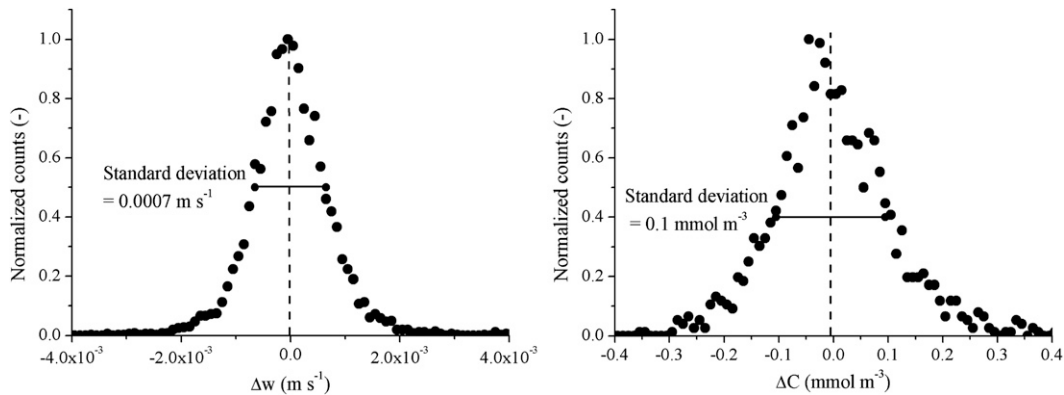


FIG. 6. Histogram of the differences between two consecutive data points of (left) vertical velocity (Δw) and (right) DO (ΔC). Both time series were low-pass filtered with a cutoff frequency of 1 s^{-1} (highest frequency expected contributing to fluxes; Table 1) before taking the difference. The standard deviations of these differences are a measure of the noise level of the two main EC components (ADV and DO electrode, including their electronics).

shown in Fig. 6. We use the standard deviation of the difference of two consecutive data points (1 s apart) as a quantitative proxy for the noise. A filter frequency of 1 Hz was selected because it is just beyond the expected smallest time scale contributing to the DO fluxes in aquatic systems (Berg et al. 2003; Table 1). Figure 7 demonstrates that reducing capacitance decreases the response time but also increases the noise. For our inland water applications, the optimal capacitance was in the range of 100 to 220 pF. This optimum needs to be chosen according to the turbulence respective noise conditions at the measurement site.

b. Data analysis for eddy flux estimations

For flux estimations, the data are treated along the steps outlined in Table 2. The individual data processing is illustrated with samples from data collected in lakes and reservoirs.

1) DESPIKING AND FILTERING

After calibrating the DO data, single-point spikes are removed by replacing the outliers with values interpolated from neighboring data points, thereby maintaining the number of samples in order not to change the time resolution and synchronization. DO spikes mainly occur because of particles hitting the sensor tip. Multipoint spikes are difficult to replace; therefore, data sections affected by multipoint spikes should not be included in EC flux calculations. Velocity spikes may be removed with the ExploreV processing software (Nortek AS, Norway) or by the interpolation method by Goring and Nikora (2002).

Noise in the two sensors, occurring independently, is usually uncorrelated and will not contribute to the flux. Correlated noise, such as wake turbulence caused, for example, by tripod legs is not easily identifiable or

removed, and therefore needs to be prevented as much as possible during measurements. Potential interference can be identified by simply comparing the current direction with the orientation of the tripod legs.

2) CALCULATION OF TURBULENT FLUCTUATIONS

The calculation of the turbulent flux with Eq. (3) requires the extraction of the recorded fluctuations w' and C' . There are three often-used procedures for estimating and removing the average reading: mean removal, linear detrending, and running averaging. The software package EddyFlux version 1.6 (P. Berg et al. 2010, unpublished manuscript) allows all three options. Mean

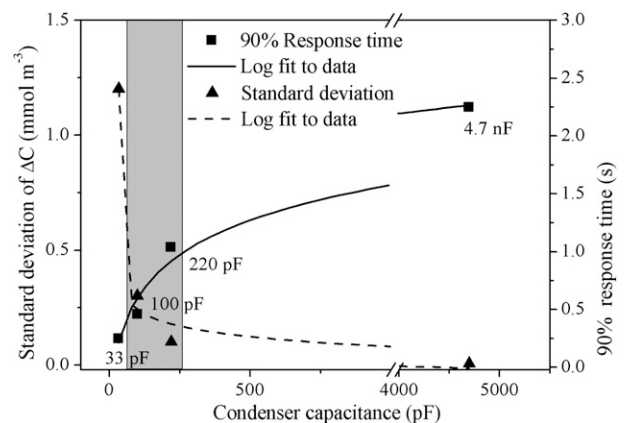


FIG. 7. Reproducibility (standard deviation of ΔC = difference of consecutive DO values; Fig. 6) determined by laboratory measurements in (left) 0% DO water and (right) sensor response time vs condenser capacitance. The DO time series are low-pass filtered by a cutoff frequency of 1 s^{-1} . The gray-marked capacitor range is suitable for EC measurements; i.e., both the sensor noise and the sensor response time are compatible with the resolution requirements (Table 1).

TABLE 2. Description the eddy correlation workflow (documented with references). The numbers indicate the order for the EC data processing.

Processing step	Specification	Reference
1) Despiking DO and current velocity signal, noise removal	Removing spikes caused by electronic noise and by particles sticking at the DO sensor. It is critical not to lose real fluctuations by filtering the spikes.	Goring and Nikora (2002)
2) Tilt correction	First, rotation into main current direction so that $\bar{u}_2 = 0$. Second, rotation to $\bar{w} = 0$.	Lee et al. (2004)
3) Calculation of turbulent fluctuations	Detrending and running averaging: subtracting the temporal averages from the recorded signals of vertical velocity and DO to extract w' and C' .	Lee et al. (2004)
4) Time-shift correction	Cross correlation of w' and C' provides the time interval by which the DO signal has to be shifted relative to the velocity signal.	Mauder and Foken (2004) McGinnis et al. (2008)
5) Calculate cospectrum	Using the cospectrum to check for turbulence break down caused by changes in flow direction or stagnant phases.	Lee et al. (2004) Mauder and Foken (2004)
6) Frequency response correction	Correction for frequency response (damping) in the covariance spectrum, before flux integration.	Eugster and Senn (1995) Horst (1997, 2000) Lee et al. (2004)
7) Calculation of DO flux	Vertical DO flux is calculated by integrating over the corrected cospectrum C_{wC} .	Berg et al. (2003, 2007) Kuwae et al. (2006) Lee et al. (2004)

removal is not recommended as it leads to a systematic overestimation or underestimation of fluxes if signals show trends (Rannik and Vesala 1999), and the appropriate extraction method (linear detrending or filtering by running averaging) depends on these trends. In our experience, data recorded in a system affected by internal waves or seiche requires filtering by running averaging. The current direction frequently changes and at the flow reversal point (velocities approach zero), turbulent transport breaks down (Brand et al. 2008). Thus, data recorded right before and after flow reversals should not be included in DO flux calculations because of nonstationarity (Lee et al. 2004; Rannik and Vesala 1999). Such a dynamic system requires filtering that removes large-scale signals over a broader frequency range. Generally, at study sites exhibiting steady unidirectional flow, the difference between linear detrending and running averaging is negligible (Fig. 8).

Filtering by running averaging requires knowledge of the appropriate averaging window length (McGinnis et al. 2008). The shape of the cumulative cospectrum reveals whether all contributing eddies were sampled by the EC device. The spectra in Fig. 9 were calculated over 14-min time series recorded in Lake Wohlen with the software Spectra 1.1 (P. Berg et al. 2010, unpublished manuscript). The integrated cospectrum (Fig. 9d) yields the total turbulent flux for that time period. At high frequencies ($>0.3 \text{ s}^{-1}$) the contributions are negligible, as the covariance represents mainly uncorrelated noise,

which cancels out by the flux integration (Fig. 9). At lower frequencies (from ~ 0.3 to $\sim 0.003 \text{ s}^{-1}$), the flux increases steeply, indicating the spectral region of the dominant contributions to the flux (Fig. 9). At even lower frequencies, the spectrum should level off indicating no further flux-contributing motions except reversible flows such as waves. The frequency at which

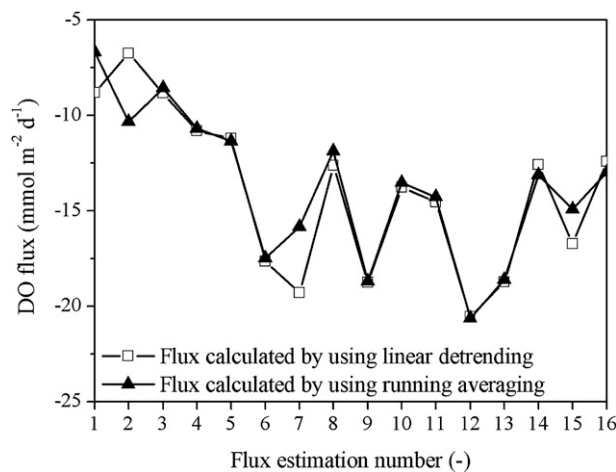


FIG. 8. Comparison of 16 flux estimates, as calculated by using both linear detrending and running averaging for the Reynolds decomposition. The individual fluxes are estimated over 14 min. The difference between the two averages over the 16 estimates (linear detrending: $-14.0 \pm 4.2 \text{ mmol m}^{-2} \text{ day}^{-1}$; running averaging: $-13.7 \pm 3.8 \text{ mmol m}^{-2} \text{ day}^{-1}$) is not significant. Data measured on 25 May 2007 in Lake Wohlen, Switzerland.

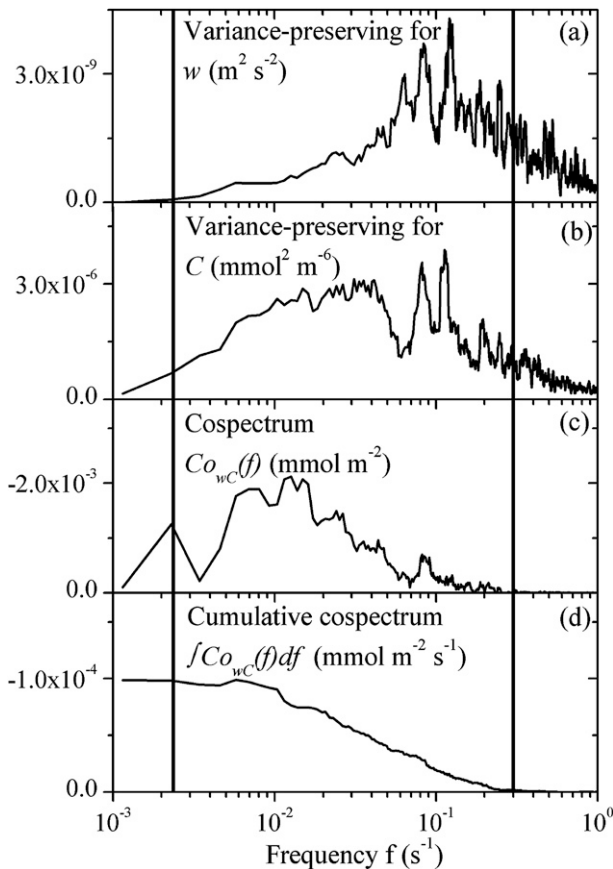


FIG. 9. Flux-contributing range marked with bold vertical lines. These boundaries are applied to variance-preserving power spectra of (a) vertical velocity w' and (b) DO concentration C' ; as well as to (c) the cospectrum of vertical velocity w' and DO fluctuations C' , and (d) to the cumulative cospectrum. For comparison, all four plots are on the same frequency scale. All spectra except (d) cumulative cospectrum were smoothed by adjacent-averaging over five data points. Data measured on 25 May 2007 in Lake Wohlen, Switzerland.

the flux levels off ($\sim 0.003 \text{ s}^{-1}$; Fig. 9) indicates the minimum window length to be used for the Reynolds decomposition. Choosing the appropriate window length is crucial, as a window that is too short could lead to an underestimation of the fluxes and one that is too long may cause overestimation of fluxes.

An alternative means to assess the appropriate window length is to stepwise increase the length and calculate the flux for each window. McGinnis et al. (2008) showed that the resulting curve follows the shape of the cospectrum (Fig. 10) and both curves reach their plateau at the low frequency range of $\sim 0.003 \text{ s}^{-1}$ resulting in a 5-min window length.

3) TIME-SHIFT AND DISTANCE CORRECTION

There is inevitably some delay in the DO signal with respect to velocity measurement due to the different

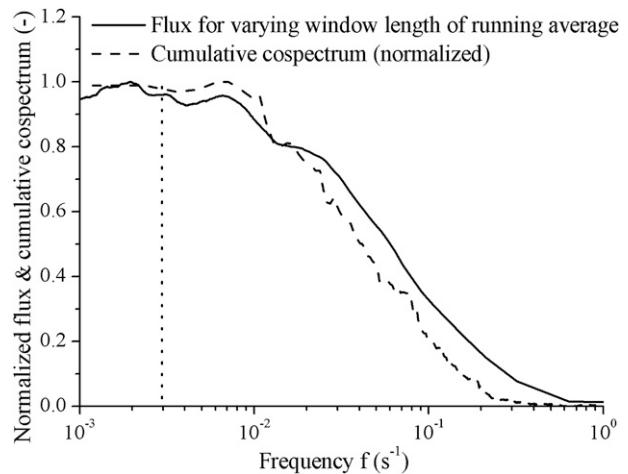


FIG. 10. Normalized cumulative cospectrum (dashed line) shows the frequency range of the flux-contributing eddies compared to the flux as calculated by stepwise increasing the window length of the running-averaging (solid line). The vertical dotted line marks the frequency chosen for filtering and the window length for running-averaging (~ 5 min), respectively. Data measured on 25 May 2007 in Lake Wohlen, Switzerland.

frequency responses. The distance between the sensor tip and the ADV sample volume also causes some time offset, depending on flow velocity and direction. By cross correlating the w' and C' fluctuations, the resultant time shift can be quantified (Fig. 11) and the two data records can be shifted relative to each other (Mauder and Foken 2004). The cumulative cospectrum would contain a time-shift-dependent but artificial flux contribution if the correction would not be applied (Fig. 11).

The time-shift correction may not be constant throughout the time series because of varying currents. Therefore, this correction should be performed on segments with approximately steady conditions. In our experience, dividing the time series into ~ 15 min sections turned out to be an appropriate duration, as explained above (Businger 1986).

4) CALCULATION OF COSPECTRUM

A common approach for computing cospectra is to use the Welch method of spectral density estimation. In MATLAB the command (csd) computes the Welch algorithm for positive frequencies. The specified Hanning window is applied to each successive detrended section and these segments are transformed with a fast Fourier transformation of a given length. For each sequence a periodogram is formed by scaling the product of the transformed w' section and the conjugate of the transformed C' section. It averages the periodograms of the successive overlapping sections to form Co_{wC} , the cross-spectral density of w' time C' . Integrating over this cospectrum yields the vertical flux ($\overline{w'C'}$).

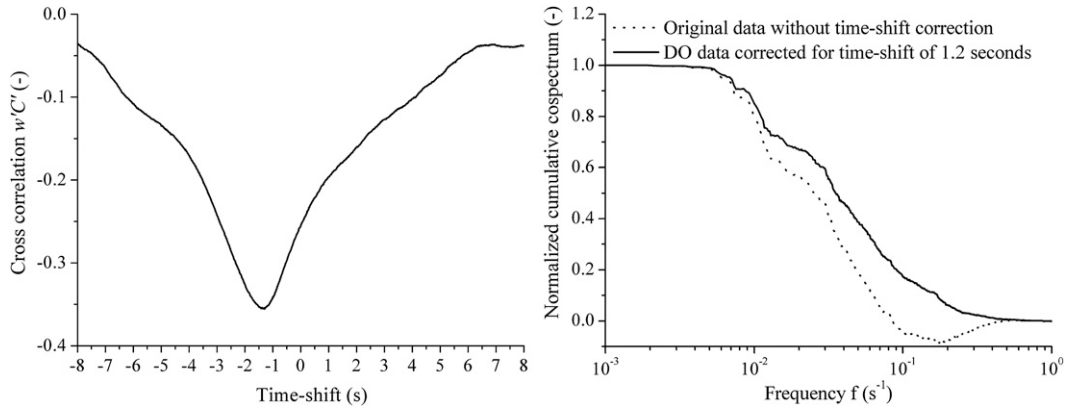


FIG. 11. (left) Cross correlation between DO fluctuations C' and vertical velocity fluctuations w' . Minimum of the curve shows time shift of the DO series relative to velocity record. (right) Time-shift corrected cumulative cospectrum (solid line) compared to the cumulative cospectrum of the original (nonshifted) data showing an artifact contribution at higher frequencies (dotted line). Data measured on 25 May 2007 in Lake Wohlen, Switzerland.

5) FREQUENCY RESPONSE CORRECTION

Correction for frequency-dependent damping is needed to compensate for the flux lost due to the finite response time of the sensor (Eugster and Senn 1995). Figure 12 shows the effect of the spectral enhancement applied to the flux-contributing range of the cumulative cospectrum by the equation $Co_{wC,corr}(f) = (1 + 4\pi^2 f^2 \tau_C^2) Co_{wC,meas}$, where $Co_{wC,meas}$ and $Co_{wC,corr}$ are the measured and corrected cospectra of $w'C'$, f is the frequency, and τ_C is the $1/e$ response time of the DO sensor (including electronics). The flux loss due to the limited frequency response τ_C of ~ 0.5 s is $\sim 10\%$ in this example (Fig. 12). Depending on the electronics used, the frequency response of the sensor, as well as on the turbulence level, the flux loss may be nearly negligible.

6) DO FLUX CALCULATION

Integrating the cospectrum $w'C'(t)$ [Eq. (4)] provides the average flux representative for the respective footprint area (Figs. 9c,d). Integration should be performed after applying corrections.

4. Simultaneous application of two EC devices in a reservoir

We deployed two physically independent EC devices utilizing the same measurement technique side by side in Lake Wohlen, Switzerland, a eutrophic run-of-river reservoir (McGinnis et al. 2008). The data were collected 25 May 2007 from 0000 to 0830 (local time) LT in ~ 1 m deep water near the shore. Mean horizontal current velocity was ~ 0.02 m s⁻¹ and mean vertical velocity ~ 0.001 m s⁻¹.

a. Devices used

Both EC devices (abbreviated by EC1 and EC2 in this section) consist of an ADV (Vector, Nortek) and a fast-responding (< 0.3 s for 90% signal) Clark-type oxygen microsensor (custom-made for EC1; fast Ox-10, Unisense for EC2). In EC1, the oxygen microsensor is connected directly to an amplifier developed at the Max Planck Institute for Marine Microbiology (Berg et al. 2003; Berg and Huettel 2008). In EC2, the oxygen sensor is connected to the amplifier (~ 1.2 s for 90% signal, section 3) by wires insulated within a paraffin-filled rubber tube.

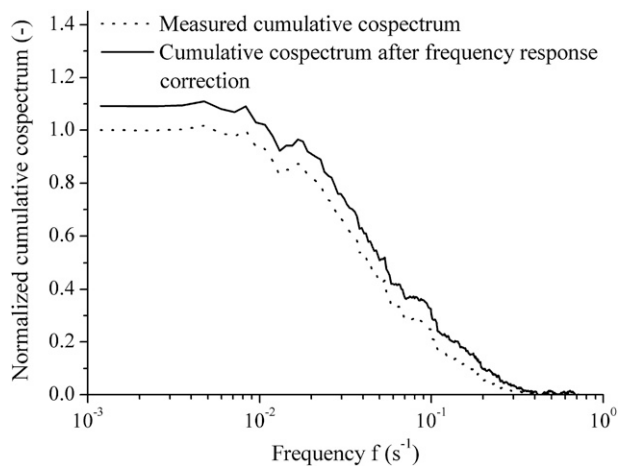


FIG. 12. Normalized cumulative cospectra shown as original spectrum (dotted line) and after frequency response correction (solid line). The correction (spectral enhancement) causes an increase in the flux of $\sim 10\%$ for a response time of 0.5 s. Data recorded 25 May 2007 in Lake Wohlen, Switzerland.

b. Deployment

The two EC devices were mounted on the same frame ~ 0.5 m apart from each other. The sensors were polarized before deployment. A temperature and DO logger (TDO-2050 RBR Ltd., Canada) was fixed on the frame leg at the same level as the oxygen microelectrodes for sensor calibration. EC1 sampled in burst mode of 14 min and EC2 sampled in continuous mode. Sampling rate was set to 64 s^{-1} for both devices.

c. Data analysis

The velocity and DO data are analyzed for fluxes using the PC software package EddyFlux Version 1.6 (P. Berg et al. 2010, unpublished manuscript). The program allows coordinate rotation to correct the velocity for instrument tilt ($\overline{w} = 0$), and turn u_1 axis into the main flow direction ($\overline{u}_2 = 0$). The data processing procedure outlined in Table 2 was used to analyze both datasets. Turbulent fluxes were derived over 14 min (burst length) time series. Both datasets were calibrated with respect to the DO logger. The flux data from EC2 have been enhanced by 10% to correct for the flux loss due to the $1/e$ sensor response of ~ 0.5 s.

d. Results

Differences between fluxes extracted with linear detrending and fluxes extracted with running averaging are negligible, hence in Fig. 13 fluxes extracted with running averaging are shown. The fluxes of both EC devices (Fig. 13) are well within a factor of 2 and reveal a pronounced diel consumption–production cycle: right after sunrise at 0540 LT, the oxygen flux changes from respiration at night (negative flux) to net production (production minus respiration) during daytime (positive flux).

A section of the DO time series from EC1 was omitted (around 0530 LT) because of excessive spikes, probably due to an object (particle) contacting the sensor tip. The DO fluxes averaged over 5 h at night (oxygen consumption) showed good agreement (EC1: flux = $-15.2 \pm 3.1 \text{ mmol m}^{-2} \text{ day}^{-1}$; EC2: flux = $-14.4 \pm 3.6 \text{ mmol m}^{-2} \text{ day}^{-1}$).

e. Discussion

The two EC devices provided consistent results. Both devices showed the same reaction in terms of consumption and production with small difference in the mean fluxes. Part of the difference between the EC1 and EC2 averages can be explained by the high variability of the DO fluxes averaged over 14 min for each EC device. The expected accuracy for an average over 14 min is only $\sim 40\%$ and even averaging over 1 h would reduce

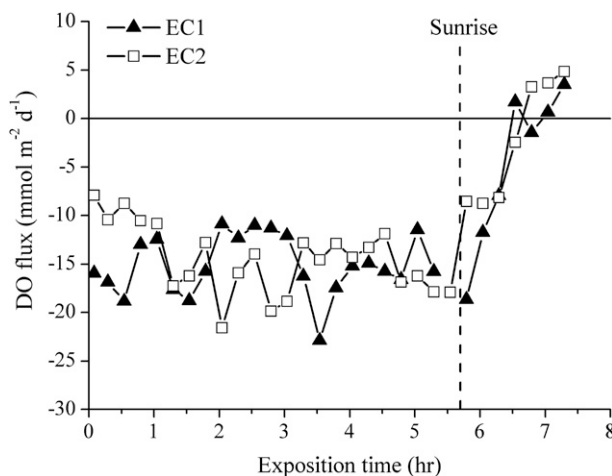


FIG. 13. Comparison of the two DO fluxes in 1-m-deep water estimated from an 8-h dataset recorded in Lake Wohlen with two completely independent EC devices deployed simultaneously. Negative DO fluxes are directed toward the sediment (consumption). Fluxes turn positive (away from the sediment, production) shortly after sunrise (dashed), which was at 0540 LT 25 May 2007.

the variability of the covariance only to $\sim 20\%$ (section 2c). Furthermore, each device covered a specific footprint (ellipse-type over which the fluxes are measured; see Berg et al. 2007 for detailed description) that overlapped between the two areas. Using the equation from Berg et al. (2007), we determined a width for one footprint (contributing 90% to the flux) of ~ 0.65 m resulting in a $\sim 20\%$ overlap of the width in our application. Thus, further small differences in the 14-min averaged fluxes are expected because of different measurement areas. This comparison provides confidence that the EC technique applied to aquatic environments is reliable and reproducible. Comparisons to other DO flux measurement approaches such as microprofiles or benthic chambers (McGinnis et al. 2008; Berg et al. 2003, 2009) led to the conclusion that the EC technique is suited for measuring DO fluxes in absolute terms.

5. Discussion and outlook

EC applied in aquatic environments is a promising new technique that allows the measurement of benthic DO fluxes in a noninvasive manner. This technique stands out from traditional, “invasive” methods such as microprofiling or chamber measurements, and takes into account the hydrodynamic regime influencing constituent transport. In addition to resolving temporal flux dynamics, a useful by-product of EC measurements is to provide insights into BBL dynamics and turbulence.

The EC instrumentation must be able to reasonably resolve the flux-relevant scales. The smallest fluctuations

listed in Table 1 require a minimum detectable difference of about $w' = 0.001 \text{ m s}^{-1}$ (low turbulence; Table 1) and $C' = 0.012 \text{ mmol m}^{-3}$ (high turbulence; Table 1), respectively. Comparing these values to the detection limits of both the ADV ($\Delta w = 0.0007 \text{ m s}^{-1}$) and the DO sensor ($\Delta \text{DO} = 0.1 \text{ mmol m}^{-3}$; Fig. 6) implies that the EC technique challenges the resolution of the two sensors. Under unfavorable conditions of especially weak turbulence or low oxygen gradients, the fluctuations may be too small to be resolved. Fortunately, the smallest fluctuations listed in Table 1 do not represent a significant contribution to the cospectrum and the major contributions to the cospectrum are from larger fluctuations.

In addition, the noise of the two signals at the smallest scales (high frequencies) is mostly uncorrelated and does not contribute to the integral of the cospectrum. Therefore, the signal-to-noise ratio of the smallest fluctuations improves by several factors only if the correlated components are considered (Goodman et al. 2006). As a result the flux-relevant resolution of the two signals is much higher, as indicated by the variance-preserving spectra of DO and vertical velocity at frequencies higher than 0.3 s^{-1} (Figs. 9a,b). Thus, the two sensors can sufficiently resolve the flux-relevant scales for a wide range of conditions in natural waters.

We tested the data analysis protocol (Table 2) by applying it to several datasets recorded in a seiche-driven lake and in a run-of-river reservoir. Averaging should be performed only over time series that are not affected by abrupt changes either in velocity or concentrations. For extracting the fluctuations from such dynamic time series, a running averaging is preferentially used, which leads to less systematic overestimation of the fluxes (Rannik and Vesala 1999; Lee et al. 2004). We found that there are negligible differences between fluxes extracted by linear detrending or running averaging for the data recorded in a riverlike reservoir with well-developed turbulence. Separation of turbulent contributions is still one of the major challenges and a source of potential errors in the flux estimates.

So far the EC technique has been applied successfully on distinct sites like rivers (Berg et al. 2003, 2007), a run-of-river reservoir (McGinnis et al. 2008), a seiche-driven lake (Brand et al. 2008), coastal sites (Berg et al. 2003, 2007), the deep sea (Berg et al. 2009), an intertidal wave affected site (Kuwaie et al. 2006) over different substrates and exposed to several hydrodynamic conditions. However, an ever increasing number of field applications and experiments will reveal the full potential of the EC technique and lead to routinely applicable measurements of fluxes in aquatic systems.

Acknowledgments. We thank A. Hume, Ch. Dinkel, M. Schurter, L. Rovelli, M. Schmid, J. Carpenter, and R. Lueck and three anonymous reviewers for their great scientific and practical advice. We are grateful to M. Begert for his statistical support. The work was financially supported by the Swiss National Science Foundation (Grants 200020-111763 and 200020-120128) and by Eawag.

REFERENCES

- Baldocchi, D. D., 2003: Assessing the eddy covariance technique for evaluating carbon dioxide exchange rates of ecosystems: Past, present and future. *Global Change Biol.*, **9**, 479–492.
- Berg, P., and M. Huettel, 2008: Monitoring the seafloor using the non-invasive eddy correlation technique: Integrated benthic exchange dynamics. *Oceanography*, **21**, 164–167.
- , H. Røy, F. Janssen, V. Meyer, B. B. Jørgensen, M. Hüttel, and D. de Beer, 2003: Oxygen uptake by aquatic sediments measured with a novel non-invasive eddy-correlation technique. *Mar. Ecol. Prog. Ser.*, **261**, 75–83.
- , —, and P. L. Wiberg, 2007: Eddy correlation flux measurements: The sediment surface area that contributes to the flux. *Limnol. Oceanogr.*, **52**, 1672–1684.
- , R. N. Glud, A. Hume, H. Stahl, K. Oguri, V. Meyer, and H. Kitazato, 2009: Eddy correlation measurements of oxygen uptake in deep ocean sediments. *Limnol. Oceanogr. Methods*, **7**, 576–584.
- Brand, A., D. F. McGinnis, B. Wehrli, and A. Wüest, 2008: Intermittent oxygen flux from the interior into the bottom boundary of lakes as observed by eddy correlation. *Limnol. Oceanogr.*, **53**, 1997–2006.
- Businger, J. A., 1986: Evaluation of the accuracy with which dry deposition can be measured with current micrometeorological techniques. *J. Climate Appl. Meteor.*, **25**, 1100–1124.
- Emerson, S., C. Stump, B. Johnson, and D. M. Karl, 2002: In situ determination of oxygen and nitrogen dynamics in the upper ocean. *Deep-Sea Res. I*, **49**, 941–952.
- Eugster, W., and W. Senn, 1995: A cospectral correction model for measurement of turbulent NO_2 flux. *Bound.-Layer Meteor.*, **74**, 321–340.
- Goodman, L., E. R. Levine, and R. G. Lueck, 2006: On measuring the terms of the turbulent kinetic energy budget from an AUV. *J. Atmos. Oceanic Technol.*, **23**, 977–990.
- Goring, D. G., and V. I. Nikora, 2002: Despiking acoustic Doppler velocimeter data. *J. Hydraul. Eng.*, **128**, 117–126.
- Gregg, M. C., 1999: Uncertainties and limitations in measuring ϵ and χ . *J. Atmos. Oceanic Technol.*, **16**, 1483–1490.
- Horst, T. W., 1997: A simple formula for attenuation of eddy fluxes measured with first-order-response scalar sensors. *Bound.-Layer Meteor.*, **82**, 219–233.
- , 2000: On frequency response corrections for eddy covariance flux measurements. *Bound.-Layer Meteor.*, **94**, 517–520.
- Kaimal, J. C., J. C. Wyngaard, Y. Izumi, and O. R. Coté, 1972: Spectral characteristics of surface-layer turbulence. *Quart. J. Roy. Meteor. Soc.*, **98**, 563–589.
- Kolmogorov, A. N., 1941: The local structure of turbulence in incompressible viscous fluid for very large Reynolds numbers. *Dokl. Akad. Nauk SSSR*, **30**, 301–305.
- Kuwaie, T., K. Kamio, T. Inoue, E. Miyoshi, and Y. Uchiyama, 2006: Oxygen exchange flux between sediment and water in an

- intertidal sandflat, measured in situ by the eddy-correlation method. *Mar. Ecol. Prog. Ser.*, **307**, 59–68.
- Lee, X., W. J. Massman, and B. E. Law, 2004: *Handbook of Micrometeorology: A Guide for Surface Flux Measurement and Analysis*. Kluwer Academic, 250 pp.
- Mauder, M., and T. Foken, 2004: Documentation and instruction manual of the eddy covariance software package TK2. Vol. 26, Universität Bayreuth, Abt. Mikrometeorologie, Arbeitsergebnisse, 44 pp.
- McGinnis, D. F., P. Berg, A. Brand, C. Lorrain, T. J. Edmonds, and A. Wüest, 2008: Measurements of eddy correlation oxygen fluxes in shallow freshwaters: Towards routine applications and analysis. *Geophys. Res. Lett.*, **35**, L04403, doi:10.1029/2007GL032747.
- Mudge, T. D., and R. G. Lueck, 1994: Digital signal processing to enhance oceanographic observations. *J. Atmos. Oceanic Technol.*, **11**, 825–836.
- Rannik, Ü., and T. Vesala, 1999: Autoregressive filtering versus linear detrending in estimation of fluxes by the eddy covariance method. *Bound.-Layer Meteorol.*, **91**, 259–280.
- Redfield, A. C., 1958: The biological control of chemical factors in the environment. *Amer. Sci.*, **46**, 205–221.
- Stull, R. B., 1988: *An Introduction to Boundary Layer Meteorology*. Kluwer Academic Publishers, 666 pp.
- Taylor, G. I., 1938: The spectrum of turbulence. *Proc. Roy. Soc. London*, **164**, 476–490.
- Van der Hoven, I., 1957: Power spectrum of horizontal wind speed in the frequency range from 0.0007 to 900 cycles per hour. *J. Atmos. Sci.*, **14**, 160–164.
- Vollenweider, R. A., 1975: Input-output models - With special reference to the phosphorus loading concept in limnology. *Schweiz. Z. Hydrol.*, **37**, 53–84.
- Wüest, A., and A. Lorke, 2003: Small-scale hydrodynamics in lakes. *Annu. Rev. Fluid Mech.*, **35**, 373–412.